WILEY | Hindawi

Research Article

Multiband Pattern Synthesis of Time-Modulated Conformal Array with Quadratic Convex Optimization Algorithm

Xiao Dong,[1] **Hailin Li** ,[1] **Ke Wang,**[1] **Yanwei Zhang,**[1] **and Yongyan Chu**[2]

[1]*Key Laboratory of Radar Imaging and Microwave Photonics, College of Electronic and Information Engineering,*
Nanjing University of Aeronautics and Astronautics, Nanjing 210016, China
[2]*Nanjing Chuhang Technology Co., Ltd., Germany*

Correspondence should be addressed to Hailin Li; nuaalhls@nuaa.edu.cn

Aiming at the multiband pattern synthesis problem of time-modulated conformal array antenna, a quadratic convex optimization algorithm is proposed for sum and difference beamforming with low sidelobe levels. This articles method synthesizes a difference beam with a low sidelobe level by generating nulls at the center frequency band and optimizing the switch-on duration time of array elements. And the sum beamforming and sidelobe suppression of the first-order sideband are realized by optimizing the switch-on instant time of the array elements. The proposed algorithm has excellent properties of sidelobe suppression and angular sweep. The simulation results of circular and satellite array antenna verify the effectiveness of the algorithm.

1. Introduction

Microsatellites have the advantages of small size, short development period, and low cost. Microsatellites are mainly used in electronic communication, remote sensing, and scientific research [1]. The spaceborne antenna is the hub of the microsatellite communication system. The design of the spaceborne antenna should not only take account into its complex working environment but also the requirements of volume and performance [2]. Therefore, the optimization design of the spaceborne antenna layout is of great significance. The geometry of the spaceborne antenna is mostly conformal array to achieve the purpose of full airspace beam coverage such as curved array [3], spherical array [4], and cylindrical array [5]. Conformal array antennas have better aerodynamic properties [6].

A modified Bernstein polynomial is introduced for the amplitude control variable, and a particle swarm optimization algorithm is used to obtain a conformal array antenna pattern with low sidelobe levels [7]. A conical wide-angle scanning conformal-phased array antenna for drone platforms is designed [8]. Although conformal array antennas have superior aerodynamic properties, conventional confor-

mal array antenna have high cross-polarization horizontal and amplitude excitation dynamic ranges. In recent years, the introduction of time modulation technique to conventional conformal arrays has been an attractive area of research. Time modulation technology refers to the introduction of time dimension in the traditional phased array, and the switching state of the array element is controlled by the radio frequency switch [9]. Multibeamforming is implemented based on a time-modulated subarray architecture. Sideband radiation is minimized by suppressing sideband level in a given static mode [10]. Aiming at the harmonic beamforming problem of time-modulated planar array, a beamforming method based on partitioned subarrays is proposed [11]. In some studies, the global optimization algorithm is applied to the synthesis and optimization of band pattern of time-modulated conformal arrays. A particle swarm optimization algorithm based on the nonlinear characteristics of radio frequency switch is used to achieve pattern synthesis for time-modulated array [12]. Jiang et al. use a differential evolution algorithm to optimize amplitude weights and time-modulated pulse widths to achieve low sidelobe pattern synthesis in the center frequency band and an optional sideband, and suppress other sideband levels

[13]. In order to minimize the sidelobe level of the nonuniform circular antenna array under the constraint of fixed beam width, genetic algorithm is used to determine the optimal weight and antenna element separation [14]. The improved invasive weed optimization method by introducing the crossover operation of the genetic algorithm is used for the harmonic beamforming of the array antenna to obtain the optimized excitation values [15]. An improved differential evolution algorithm (IDE) is used for sidelobe level synthesis and optimization of time-modulated circular array antenna [16]. A new differential evolution method is used for pattern synthesis of time-modulated planar array, which achieves high directivity and low sidelobe pattern synthesis and reduces the complexity of large-scale array antenna feed networks [17]. To solve the problem of antenna excitation optimization, a harmonic search algorithm and particle swarm optimization algorithm for concentric ring antenna array are proposed, which achieve wide uniform power density and reduce the complexity of satellite antenna system hardware [18]. The above research effectively solves the beamforming problem of time-modulated arrays. However, the swarm intelligence global optimization algorithms have high complexity and are easy to fall into the local optimal solution when solving the problem of large-scale conformal array pattern synthesis. It is possible to effectively improve the synthesis efficiency by transforming the pattern synthesis problem of the time-modulated conformal array into a convex problem since the local optimal solution of the convex optimization (CVX) problem is the global optimal solution. Hong et al. use two different solutions for convex relaxation of nonconvex problems and realized the beam pattern of phased array [19]. Zhang et al. use a quadratic Taylor expansion to make the nonconvex problem of maximizing the directivity coefficient into convex problem and use a two-stage convex iteration for sidelobe constraints [20]. An efficient method for near-field sparse array synthesis based on Bayesian compressed sensing and convex optimization is presented [21]. Prisco and D'Urso solve the synthesis problem of maximum sparse linear array based on minimization-weighted L1 norm and sequential convex optimization algorithm [22]. A convex optimization based directional pattern synthesis algorithm of radiation focused sparse array is proposed, which finally achieves sparse linear array and planar array with fewer elements and lower maximum sidelobe level [23]. The beam pattern synthesis problem is transformed into a relaxed convex optimization problem, and a sequential convex optimization algorithm is used to solve the relaxed convex optimization problem to realize beam pattern synthesis [24]. Aiming at the synthesis problem of four-dimensional antenna array, pattern synthesis is carried out based on the sequential convex optimization algorithm by suppressing range ambiguity without increasing azimuth ambiguity and system complexity [25]. For the synthesis problem of four-dimensional array antenna, an iterative convex optimization algorithm is proposed to suppress multiple sideband levels while performing beamforming at the center frequency [26]. A frequency-invariant nonuniform linear array and planar array synthesis method is proposed

to obtain the array excitation weights for all frequency sampling points through weighted convex optimization [27]. A system-driven convex algorithm is proposed for pattern synthesis of uniform amplitude and irregular planar phased array, which is capable of multibeam optimization [28]. These studies use convex optimization algorithm to efficiently achieve beamforming and sidelobe suppression. However, the above convex optimization work does not discuss the multiband pattern synthesis problem of time-modulated conformal array antenna.

In this paper, a multiband pattern synthesis algorithm for time-modulated conformal array is proposed. The quadratic convex optimization algorithm solves the problem that the amplitude excitation is difficult to control when the traditional conformal array is synthesized. And the multiband pattern synthesis is divided into the main frequency band and the first-order sideband beam synthesis to realize the utilization of arbitrary sideband and suppression of the maximum sidelobe level.

The paper is organized as follows: Section 2 presents the optimized model for multiband pattern synthesis of time-modulated conformal array. Section 3 describes how to solve the optimization model using a quadratic convex optimization algorithm. Section 4 verifies the effectiveness of the proposed method in the pattern synthesis of time-modulated conformal array by numerical analysis, realizes the multiband pattern synthesis of circular and spaceborne conformal array, and discusses the angular scanning characteristics of conformal array antenna. Finally, the conclusions are drawn in Section 5.

2. Mathematical Model

As shown in Figure 1. Conformal array is a three-dimension antenna composed by N array elements arbitrarily arranged. The conformal array introduces a switching function $u_n(t)$ for time modulation. Without considering the mutual coupling of the array elements [29, 30], the far-field radiation intensity of the time-modulated conformal array is
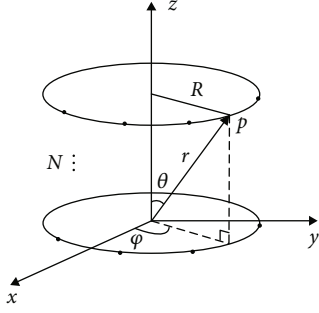
$$\boldsymbol{E}(\boldsymbol{r}, t) = \sum_{n=1}^{N} w_n u_n(t) \boldsymbol{E}_n(\boldsymbol{r}) \, e^{jK_0 \boldsymbol{p}_n^T \boldsymbol{r}} e^{j2\pi f_0 t}, \qquad (1)$$

where $u_n(t)$ is the switching function, the radiation direction of the array is $\boldsymbol{r} = [\sin \theta \cos \varphi \ \sin \theta \sin \varphi \ \cos \theta]^T$, θ is the elevation angle, and φ is the azimuth angle. w_n is the complex excitation coefficient, and $\boldsymbol{E}_n(\boldsymbol{r})$ is the radiated electric field vector. In $K_0 = 2\pi/\lambda$, λ is the wavelength of incident wave. $\boldsymbol{p}_n$ is the position vector of the n-th element, $\boldsymbol{p}_n = [x_n \ y_n \ z_n]^T$.

The radiation characteristics of the elements in the conformal array are anisotropic. The radiated electric field vector of the n-th element in the array global coordinate system (x, y, z) can be expressed as

$$\boldsymbol{E}_n(\boldsymbol{r}) = f(\Delta_n)\boldsymbol{e}_n = f(\Delta_n)[\cos (\gamma_n)\boldsymbol{e}_V + \sin (\gamma_n)\boldsymbol{e}_H], \qquad (2)$$

where $f(\Delta_n)$ is the electric field of the n-th element, $\Delta_n =$

FIGURE 1: Conformal array of N elements.

FIGURE 2: Array global and array element coordinate system.

arccos $(\boldsymbol{d}_n \odot \boldsymbol{r}) = $ arccos $(\boldsymbol{d}_n^T \boldsymbol{r})$ is the angle between the normal vector $\boldsymbol{d}_n$ of the array element and the radiation direction $\boldsymbol{r}$. $\boldsymbol{e}_n = \cos(\gamma_n)\boldsymbol{e}_V + \sin(\gamma_n)\boldsymbol{e}_H$ is the direction of the electric field. The vertical polarization direction vectors is $\boldsymbol{e}_V = [\cos\theta\cos\varphi \ \cos\theta\sin\varphi - \sin\theta]^T$. The horizontal polarization direction vectors are $\boldsymbol{e}_H = [-\sin\varphi \ \cos\varphi \ 0]^T$, respectively, which satisfy the Ampere's Law $\boldsymbol{e}_V \otimes \boldsymbol{e}_H = \boldsymbol{r}$. γ_n is the array polarization direction coefficient, satisfying

$$\cos(\gamma_n) = \cos(\gamma'_n)\left(R_n \boldsymbol{e}'_{nV}\right)^T \boldsymbol{e}_V + \sin(\gamma'_n)\left(R_n \boldsymbol{e}'_{nH}\right)^T \boldsymbol{e}_V,$$

$$\sin(\gamma_n) = \cos(\gamma'_n)\left(R_n \boldsymbol{e}'_{nV}\right)^T \boldsymbol{e}_H + \sin(\gamma'_n)\left(R_n \boldsymbol{e}'_{nH}\right)^T \boldsymbol{e}_H.$$

$$(3)$$

In the formula,

$$R_n = \begin{bmatrix} \cos\partial_n\cos\phi_n & -\sin\phi_n & \sin\partial_n\cos\phi_n \\ \cos\partial_n\sin\phi_n & \cos\phi_n & \sin\partial_n\cos\phi_n \\ -\sin\partial_n & 0 & \cos\partial_n \end{bmatrix}, \quad (4)$$

is the conversion relationship between the radiation direction $\boldsymbol{r}$ of the array global coordinate system and the radiation direction $\boldsymbol{r}'_n$ of the array element coordinate system (x', y', z'). ∂_n and ϕ_n are the radiation elevation angle and azimuth angle of the normal vector $\boldsymbol{d}_n$ of the array element, respectively.

In the array element coordinate system (x', y', z'), the array element polarization direction coefficient is γ'_n. $\boldsymbol{e}'_n = \cos(\gamma'_n)\boldsymbol{e}'_{nV} + \sin(\gamma'_n)\boldsymbol{e}'_{nH}$ is the electric field direction of n-th element. $\boldsymbol{e}'_{nV}, \boldsymbol{e}'_{nH}$ are the vertical and horizontal polarization direction vectors of the array element, respectively, and $\boldsymbol{e}'_{nV} \otimes \boldsymbol{e}'_{nH} = \boldsymbol{r}'_n$. γ_n can be obtained by Equation (3). The array global coordinate system and the array element coordinate system are shown in Figure 2.

The conformal array introduces the switching function $u_n(t)$ with modulation period T_r. The time-modulated conformal array can control the radiation characteristics through the radio frequency switch, as shown in Figure 3.

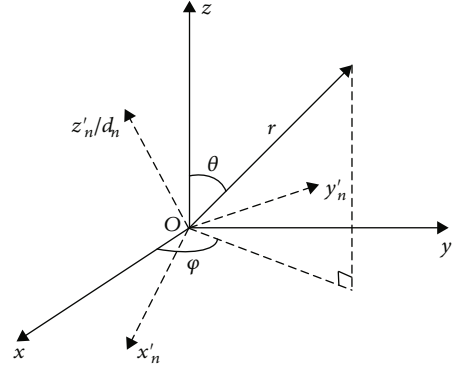$$u_n(t) = \varepsilon(t - t_n) - \varepsilon[t - (t_n + \tau_n)], \quad (5)$$
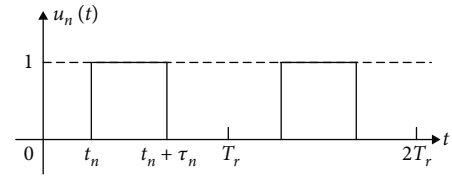

FIGURE 3: Switch function of ratio frequency switch.

where t_n is the switch-on instant time and τ_n is the switch-on duration time.

Equation (5) is transformed from the time domain to the frequency domain by Fourier transform.

$$u_n(t) = \sum_{m=-\infty}^{\infty} \tau_n f_r \operatorname{sinc}(\pi m \tau_n f_r) e^{-jm\pi f_r(2t_n + \tau_n)} e^{j2\pi m f_r t}, \quad (6)$$

where $f_r = 1/T_r$ is the modulated frequency and $m = 0, \pm 1, \cdots$ Denoting $\alpha_n = \tau_n f_r$, $\beta_n = t_n f_r$ $(0 \le \alpha_n, \beta_n \le 1)$, we get

$$u_n(t) = \sum_{m=-\infty}^{\infty} \alpha_n \operatorname{sinc}(\pi m \alpha_n) e^{-jm\pi(2\beta_n + \alpha_n)} e^{j2\pi m f_r t}. \quad (7)$$

From Equation (2) and Equation (7), we get Equation (8), where $e^{j2\pi(f_0 + m f_r)t}$ is abbreviated.

$$E(\boldsymbol{r}) = \sum_{m=-\infty}^{\infty} \sum_{n=1}^{N} \alpha_n w_n f(\Delta_n)[\cos(\gamma_n)\boldsymbol{e}_V + \sin(\gamma_n)\boldsymbol{e}_H]$$
$$\times \operatorname{sinc}(\pi m \alpha_n) e^{-jm\pi(2\beta_n + \alpha_n)} e^{jK_0 \boldsymbol{p}_n^T \boldsymbol{r}}. \quad (8)$$

Then, the far-field radiation intensity of the time-modulated conformal array in the vertical polarization direction is

$$E_V(\boldsymbol{r}) = \sum_{m=-\infty}^{\infty} \sum_{n=1}^{N} \alpha_n w_n f(\Delta_n) \cos(\gamma_n)\boldsymbol{e}_V$$
$$\times \operatorname{sinc}(\pi m \alpha_n) e^{-jm\pi(2\beta_n + \alpha_n)} e^{jK_0 \boldsymbol{p}_n^T \boldsymbol{r}}. \quad (9)$$

In order to deal with the pattern synthesis problem of multiband, we decompose the radiation intensity of the time-modulated conformal array into the main frequency

band f_0 and multiorder sideband $f_0 + mf_r$ and obtain the far-field radiation intensity of the central frequency band and multiorder sideband $E_{V0}(r), E_{Vm}(r)$, which are expressed as follows:

$$E_{V0}(r) = \sum_{n=1}^{N} \alpha_n w_n \cos(\gamma_n) f(\Delta_n) e^{jK_0 p_n^T r}, \qquad (10)$$

$$E_{Vm}(r) = \sum_{m=-\infty}^{\infty} \sum_{n=1}^{N} \alpha_n w_n \cos(\gamma_n) f(\Delta_n) \text{ sinc}(\pi m \alpha_n) e^{-j\pi m(2\beta_n + \alpha_n)} e^{jK_0 p_n^T r}. \tag{11}$$

This paper discusses the multiband pattern synthesis of the time-modulated conformal array in the vertical polarization direction. The goals of synthesis are (1) achieving maximum power radiation in a given direction in two different frequency bands. (2) Sidelobe level at the center frequency and the first-order sideband is less than the constraint $\varepsilon_1, \varepsilon_2$. Then, the mathematical model of multiband pattern synthesis is as follows:

$$\begin{aligned} \min_{w,\alpha,\beta} \quad & \varepsilon_1, \varepsilon_2 \\ s.t. \quad & E_{V0}(r_0) = 0 \\ & E_{V1}(r_1) = 1 \\ & E_{V0}(r_2) = 1 \\ & E_{V0}(r_3) = 1 \\ & E_{V0}(r_s) \leq \varepsilon_1, r_s \in \Omega_s \\ & E_{V1}(r_d) \leq \varepsilon_2, r_d \in \Omega_d \\ & 0 \leq \alpha_n, \beta_n \leq 1 \end{aligned} \qquad (12)$$

where w, α, β is the time modulation parameter, $w = [w_1 \cdots w_N]^T$ is the complex excitation coefficient, $\alpha = [\alpha_1 \cdots \alpha_N]^T$ and $\beta = [\beta_1 \cdots \beta_N]^T$ are the time modulation parameter, respectively. $E_{V0}(r_0)$ is the radiation intensity in the direction of r_0 at the center frequency band, and ε_1 is the sidelobe constraint parameter at the center frequency band. $E_{V1}(r_1)$ is the radiation intensity in the radiation direction r_1 at the first-order sideband, and ε_2 is the sidelobe constraint parameter at the first-order sideband. $E_{V0}(r_2)$ and $E_{V0}(r_3)$ are the radiation intensities in the direction of θ_1 and θ_2 at the center frequency band, respectively. $E_{V0}(r_s)$ and $E_{V1}(r_d)$ are the radiation intensities at the center frequency band and the sidelobe region Ω_s, Ω_d in the first sideband, where the sampling directions are r_s and r_d, respectively.

3. Quadratic Convex Optimization Algorithm

This paper proposes a quadratic convex optimization method to solve the mathematical model in Equation (12). The method can realize the multiband pattern of the time-modulated conformal array at the center frequency and first-order sideband. The implementation of quadratic convex optimization algorithm is divided into the following two steps.
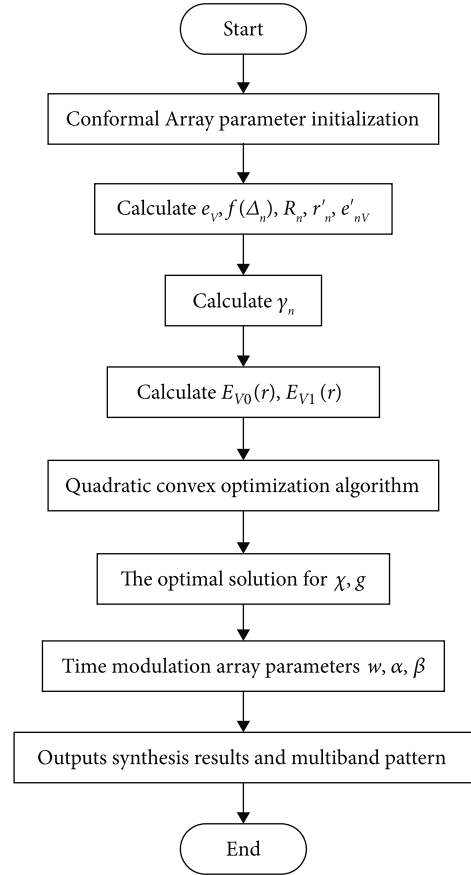

FIGURE 4: Flow chart of the proposed algorithm.

Firstly, this paper solves the synthesis problem of pattern synthesis at the central frequency band. When $m = 0$, from Equation (10), we can get that the vertical polarization electric field radiation intensity $E_{V0}(r)$ at the center frequency band is only related to the complex excitation coefficient vector w and the normalized switch turn-on duration α. Denoting $\chi = [w_1 \alpha_1 \cdots w_N \alpha_N]^T = w \cdot \alpha$ is the time complex excitation vector, and then, $E_{V0}(r)$ can be expressed as

$$E_{V0}(r) = \chi^T b_{V0}, \qquad (13)$$

where $b_{V0} = [\cos(\gamma_1) f(\Delta_1) e^{jK_0 p_1^T r_0} \cdots \cos(\gamma_n) f(\Delta_n) e^{jK_0 p_n^T r_0}]$ is the array steering vector at the center frequency band. In Equation (12), the optimal expression for the beam pattern synthesis problem of the center frequency band is

$$\begin{aligned} \min_{\chi} \quad & \varepsilon_1 \\ s.t. \quad & \chi^T b_{V0} = 0 \\ & \chi^T b_2 = 1 \\ & \chi^T b_3 = 1 \\ & |\chi^T b_{Vs}| \leq \varepsilon_1, r_s \in \Omega_s \end{aligned} \qquad (14)$$

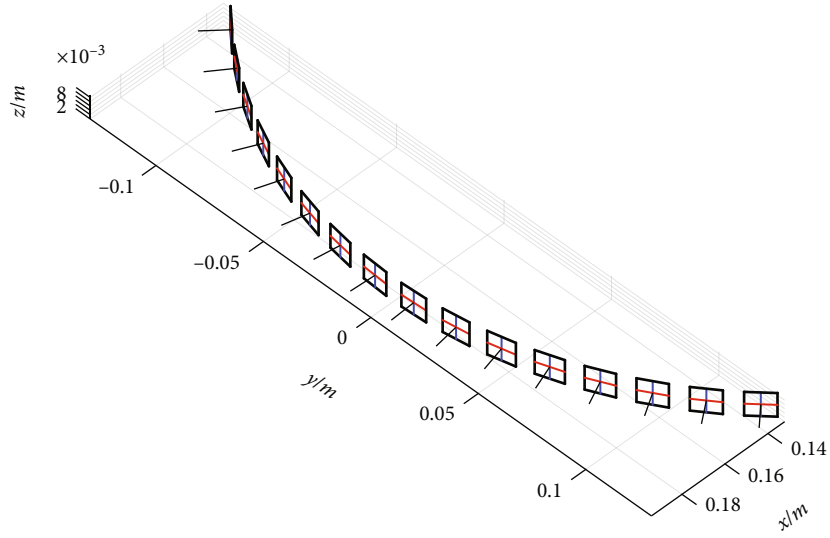where $b_{Vs} = [\cos(\gamma_1) f(\Delta_1) e^{jK_0 p_1^T r_s} \cdots \cos(\gamma_n) f(\Delta_n) e^{jK_0 p_n^T r_s}]$
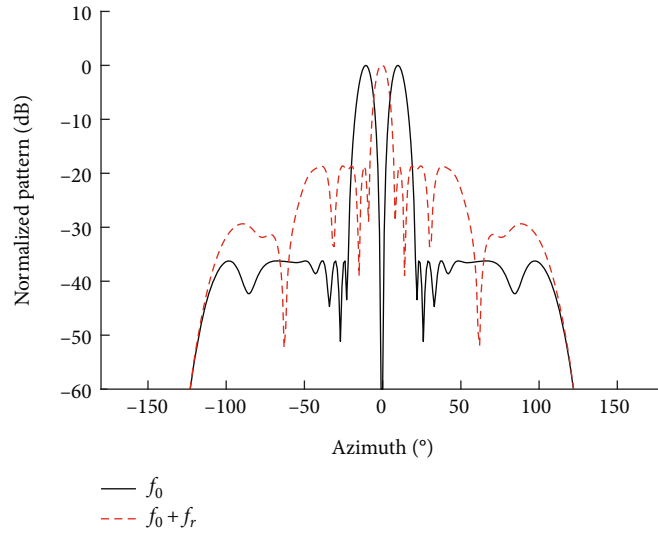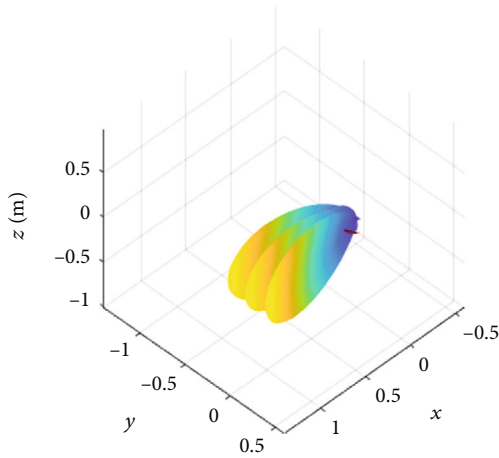
FIGURE 5: Circular array antenna layout with 16 elements.

FIGURE 6: Synthesis pattern of the circular array ($\varphi = 0°, \theta = 90°$).

FIGURE 7: 3D pattern of the circular array when $\varphi = 0°, \theta = 90°$.

TABLE 1: Pattern parameters for different algorithms.

| σ_1	IDE	CVX
SLL^0/dB	-19.81	-36.25
SLL^1/dB	-20.74	-18.71
SBL^0/dB	-1	0
BW^0/°	20	20
BW^1/°	18	10
CPU time/min	408.25	0.84 s

is the steering vector of the center frequency band. $\boldsymbol{b}_2, \boldsymbol{b}_3$ are the steering vectors in the beam direction θ_2, θ_3 of the center frequency band, respectively, and ε_1 is the sidelobe suppression parameter at the center frequency band.

TABLE 2: Timing switch sequence of time-modulated circular array.

N	α_n	β_n	N	α_n	β_n
1	0.0078	0.4023	9	0.6259	0.8077
2	0.0078	0.4553	10	0.0078	0.0634
3	0.2277	0.3957	11	0.0078	0.7373
4	0.3783	0.4336	12	0.0078	0.6300
5	0.0078	0.6299	13	0.3781	0.4338
6	0.0078	0.7366	14	0.2279	0.3956
7	0.0078	0.0634	15	0.0078	0.4555
8	0.6252	0.8079	16	0.0078	0.4023
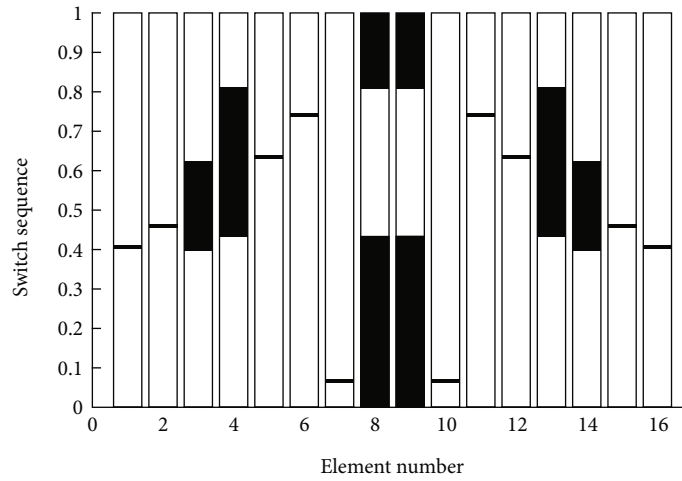
(a)
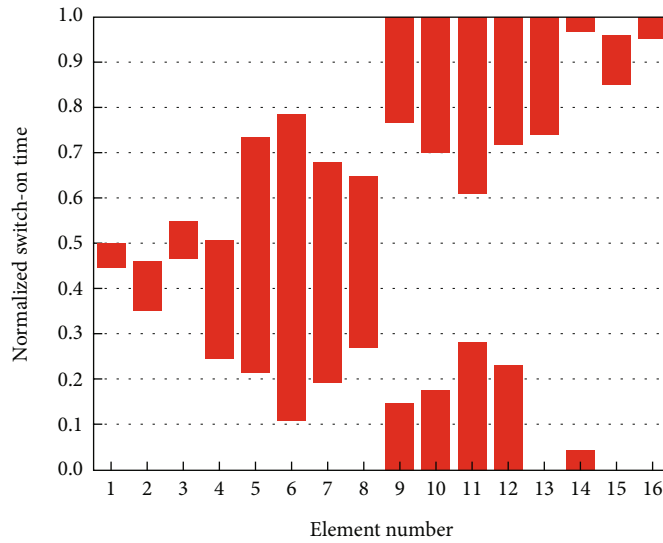
(b)

FIGURE 8: Time series of (a) proposed method and (b) IDE method.

Equation (14) is a linear programming problem, using a convex optimization algorithm to optimize the pattern of center frequency band and suppress the side lobe level. A vector χ can be found using convex optimization methods.

Then, this paper solves the synthesis problem of pattern synthesis at the first-order sideband. When $m \neq 0$, from the Equation (11), the vertical polarization electric field radiation intensity $E_{Vm}(r)$ at the sideband is related to $w_n \alpha_n$ sinc $(\pi m \alpha_n)e^{j\pi m(2\beta_n + \alpha_n)}$, which is a nonlinear complex vector and cannot
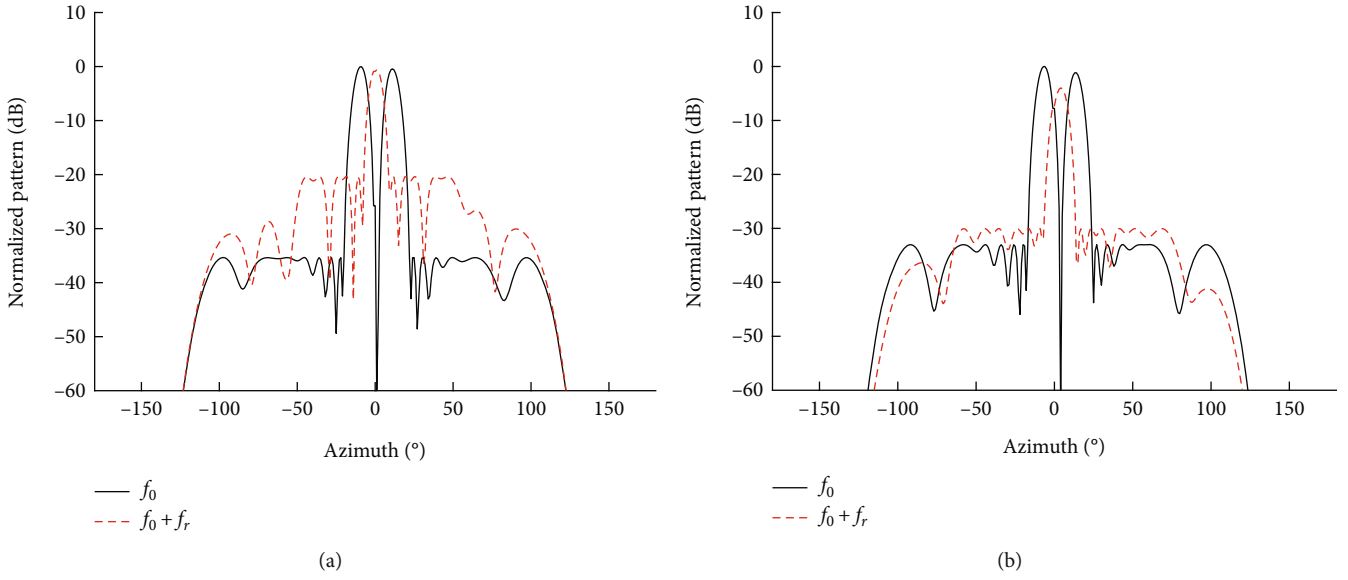
FIGURE 9: Multiband pattern in (a) $\varphi = 1°$ and (b) $\varphi = 4°$.

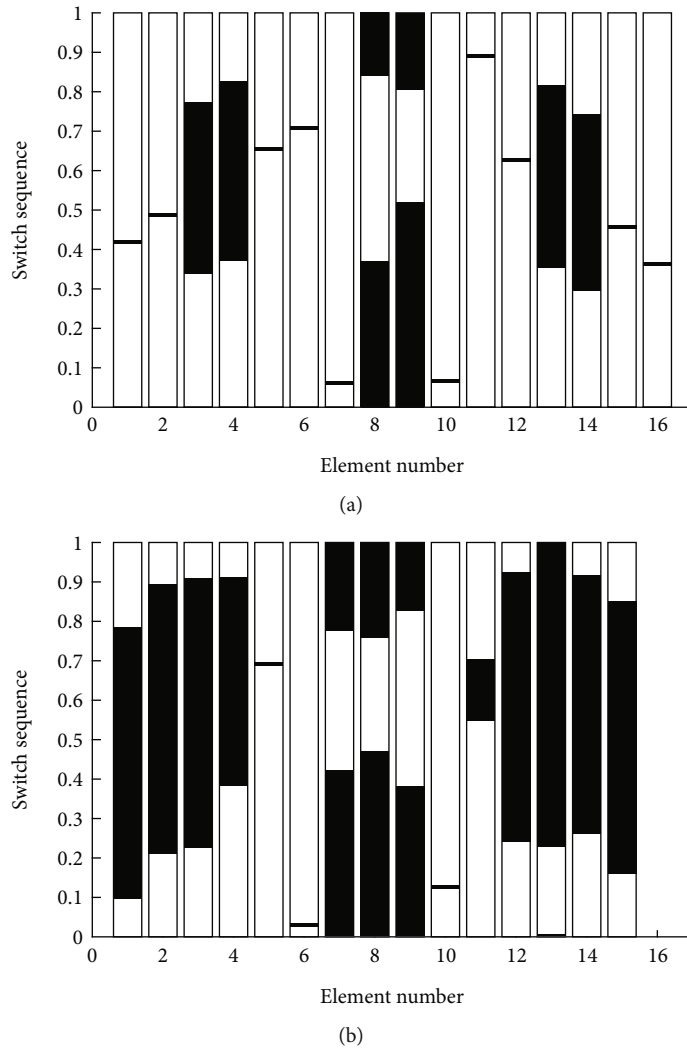FIGURE 10: Time series of (a) $\varphi = 1°$ and (b) $\varphi = 4°$.

be solved directly by using the convex optimization. When $m = 1$, denoting the partial coefficient term $g_n = \operatorname{sinc}(\pi\alpha_n) e^{-j\pi(2\beta_n+\alpha_n)}$, then, the vertical polarization electric field radiation intensity of first-order sideband is

$$E_{V1}(\boldsymbol{r}) = (\boldsymbol{\chi}\cdot\boldsymbol{g})^T\boldsymbol{b}_{V1}, \tag{15}$$

where $\boldsymbol{b}_{V1} = [\cos(\gamma_1)f(\Delta_1)e^{jK_0\boldsymbol{p}_1^T\boldsymbol{r}_1} \cdots \cos(\gamma_n)f(\Delta_n)e^{jK_0\boldsymbol{p}_n^T\boldsymbol{r}_1}]$ is the array steering vector at the first-order sideband. In Equation (12), the optimal expression for the beam pattern synthesis problem of the first-order sideband is

$$\begin{aligned} \min_{\boldsymbol{g}} \quad & \varepsilon_2 \\ s.t. \quad & (\boldsymbol{\chi}\cdot\boldsymbol{g})^T\boldsymbol{b}_{V1} = 1 \\ & (\boldsymbol{\chi}\cdot\boldsymbol{g})^T\boldsymbol{b}_{Vd} \leq \varepsilon_2, \boldsymbol{r}_d \in \Omega_d \\ & |\boldsymbol{g}| < 1 \end{aligned} \tag{16}$$

where $\boldsymbol{b}_{Vd} = [\cos(\gamma_1)f(\Delta_1)e^{jK_0\boldsymbol{p}_1^T\boldsymbol{r}_d} \cdots \cos(\gamma_n)f(\Delta_n)e^{jK_0\boldsymbol{p}_n^T\boldsymbol{r}_d}]$ is the array steering vector at the first-order frequency band, $\boldsymbol{g} = [g_1 \cdots g_N]^T$ is the unknown optimization variable, $|\boldsymbol{g}|$ is the modulus of the complex vector $\boldsymbol{g}$, and ε_2 is the sidelobe suppression parameter at the first-order sideband frequency.

From Equation (16), we can find that the pattern synthesis problem of first-order sideband also becomes a linear programming problem through deformation, which can be solved by convex optimization method to obtain the vector $\boldsymbol{g}$ that satisfies the condition. Pattern synthesis of vertically polarized electric field radiation of first-order sideband is realized by convex optimization algorithm. The pattern has maximum power radiation and sidelobe suppression.

The quadratic convex optimization algorithm solves the multiband pattern synthesis problem of time-modulated conformal array at the center frequency band and the first-order sideband, respectively. And obtaining the corresponding time-modulated array parameters $\boldsymbol{w}, \boldsymbol{\alpha}, \boldsymbol{\beta}$ by

$$\alpha_n = \frac{1}{\pi}\sin^{-1}(|g_n|),$$

$$\beta_n = -\frac{1}{2\pi}[\operatorname{angle}(g_n) + \alpha_n + 2\pi p], \forall p, 0 \leq \beta_n \leq 1, \tag{17}$$

$$w_n = \frac{\chi_n}{\alpha_n}.$$

The proposed method achieves the pattern synthesis of the center frequency band and the first-order sideband with maximum power radiation and sidelobe suppression in given direction.

The multiband pattern synthesis process of time-modulated conformal array based on quadratic convex optimization algorithm is shown in Figure 4.

(1) Initialize the conformal array, set the number of array elements N, the position of the array element $\boldsymbol{p}_n^T$, the
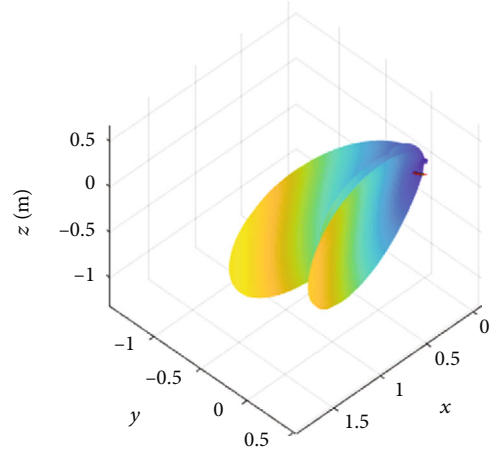

FIGURE 11: 3D pattern of the circular array when $\varphi = 4°, \theta = 90°$.

TABLE 3: Multiband pattern parameters when changing φ.

$\varphi/°$	1	2	3	4	5	6
SLL^0/dB	-35.37	-36.39	-34.68	-33.02	-34.53	-33.02
SLL^1/dB	-20.4	-22.2	-23.95	-30.06	-34.15	-42.4

center frequency f_0, the radiation direction $\boldsymbol{r}$, the polarization direction coefficient γ'_n, and the normal vector of the array element $\boldsymbol{d}_n$

(2) Calculate the vertical polarization direction vector $\boldsymbol{e}_V$ of the array according to the radiation direction $\boldsymbol{r}$, and according to the radiation direction $\boldsymbol{r}$ and the normal vector of the array element $\boldsymbol{d}_n$, calculate the included angle Δ_n and the radiation value $f(\Delta_n)$

(3) Calculate the transformation matrix $\boldsymbol{R}_n$ according to the depression angle ∂_n and azimuth angle ϕ_n of the normal vector of the array element $\boldsymbol{d}_n$. The array element coordinate system $\boldsymbol{r}'_n$ is calculated by the radiation direction $\boldsymbol{r}$ and the transformation matrix $\boldsymbol{R}_n$

(4) Calculate the vertical polarization direction vector $\boldsymbol{e}'_{nV}$ of the array element according to the radiation direction $\boldsymbol{r}'_n$ of the array element coordinate system

(5) Calculate γ_n according to the polarization direction coefficient γ'_n of the known array element

(6) Obtain the electric field strength $E_{V0}(\boldsymbol{r}), E_{V1}(\boldsymbol{r})$ of the time-modulated conformal array in the main radiation direction $\boldsymbol{r}_0, \boldsymbol{r}_1$

(7) The optimal solution of $\boldsymbol{\chi}, \boldsymbol{g}$ is obtained by quadratic convex optimization algorithm

(8) Find the time modulation array parameters $\boldsymbol{w}, \boldsymbol{\alpha}, \boldsymbol{\beta}$.

4. Simulation Results

4.1. Simulation of Circular Array Antenna. In order to verify the correctness and effectiveness of the quadratic convex
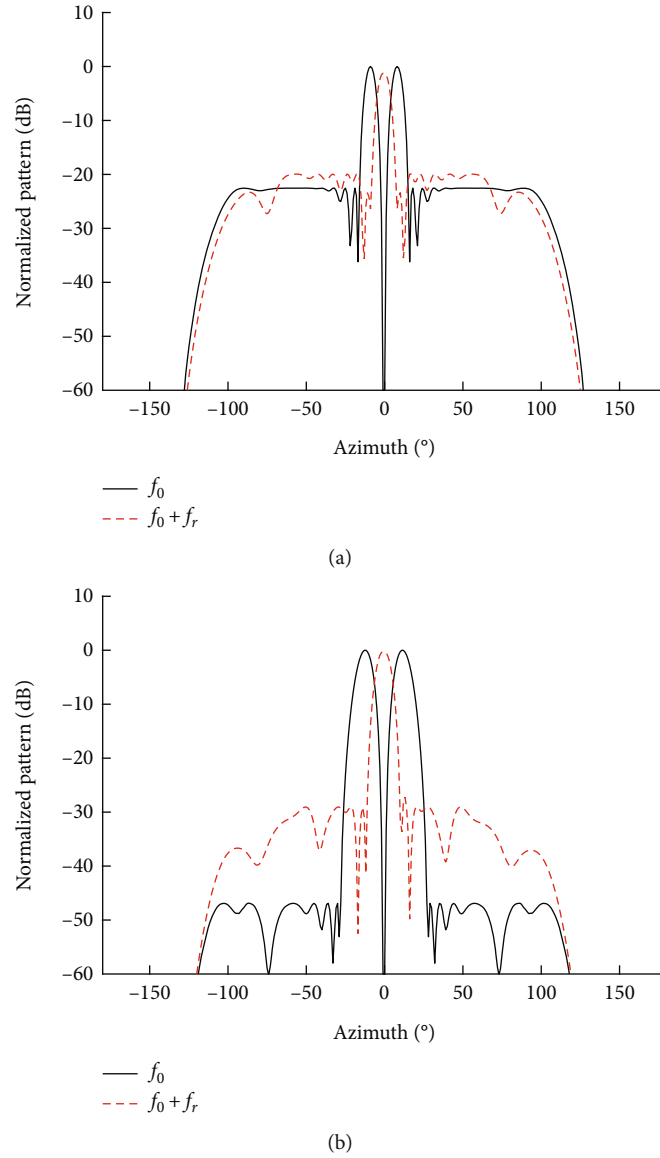
(a)

(b)

FIGURE 12: Multiband pattern when (a) BW = 7° and (b) BW = 13°.

optimization algorithm in multiband pattern synthesis of time-modulated conformal array, under the condition that the center frequency f_0 = 10GHz, the multiband pattern synthesis of the circular array antenna is considered in this paper.

4.1.1. Design of 16-Element Circular Array. The circular array is composed of 16 array elements arranged at $\lambda/2$ equal intervals. The array wavelength is λ = 0.03m. The straight line segment on the array element represents the normal vector direction of the array element, and the normal vector of all array elements is outward from the center of the ring. The layout of the 16-element circular array antenna is shown in Figure 5.

4.1.2. Multiband Pattern Performance Analysis. The main radiation direction of the initialized circular array antenna is $\varphi = 0°, \theta = 90°$. The quadratic convex optimization algorithm is used to realize the multiband pattern synthesis of

the 16-element circular array antenna. The optimized main band beamwidth is 20°, and the maximum sidelobe peak level is -36.25 dB. The first-order sideband beamwidth is 10°, and the maximum sidelobe peak level is -18.71 dB. The two-dimension pattern is shown in Figure 6. The energy radiated by the circular array antenna is concentrated in the main direction, and the sidelobe level of the antenna is suppressed, as shown in Figure 7.

In order to reflect the superiority of the quadratic convex optimization algorithm in improving the comprehensive performance of the multiband pattern of the time-modulated conformal array, this paper compares the pattern parameters results synthesized by IDE [16]. Numerical results of 16-element circular array antenna pattern synthesis of different methods are shown in Table 1.

The proposed multiband pattern synthesis result based on quadratic convex optimization algorithm has low sidelobe level and faster synthesis speed. After optimized by
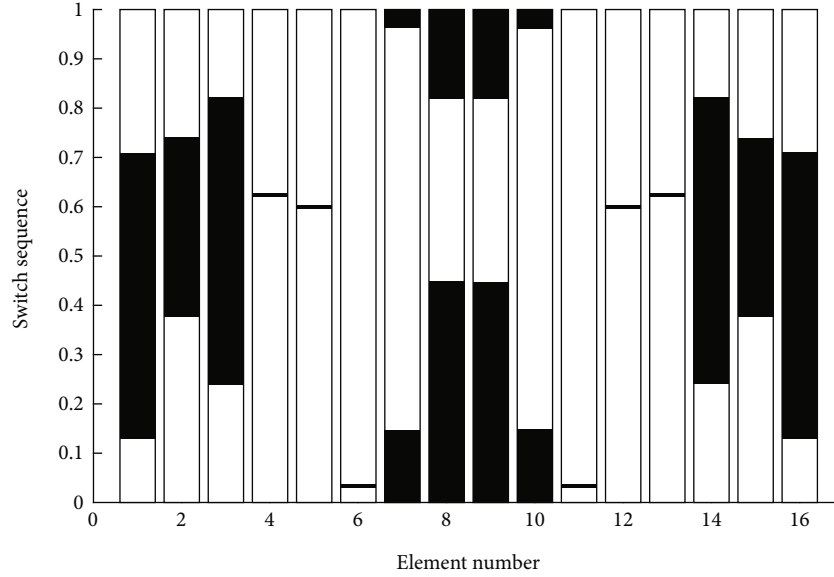
(a)
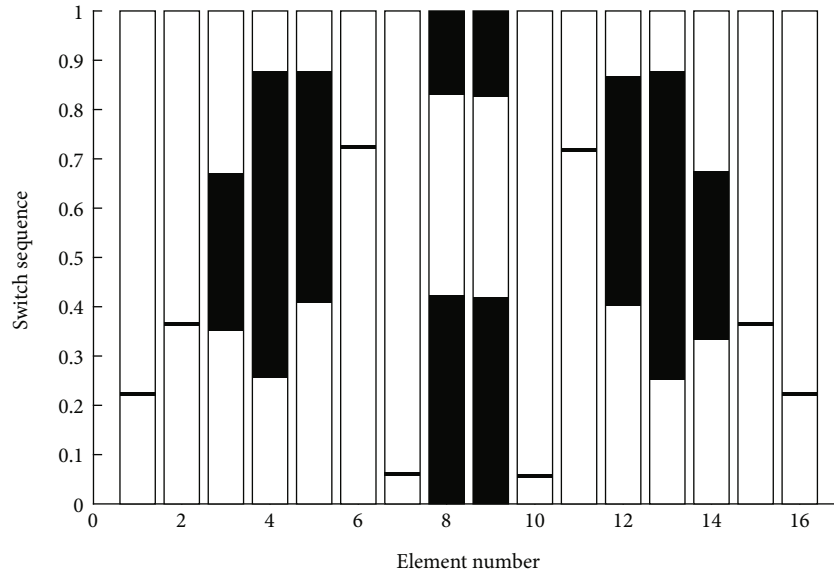
(b)

Figure 13: Time series of (a) BW = 7° and (b) BW = 13°.

quadratic convex method, the peak sidelobe level of the main frequency band is -36.25 dB. Compared with IDE algorithm, the peak sidelobe level decreased by 16.44 dB.

Comparing the complexity of the proposed method and IDE algorithm from the pattern synthesis time, the proposed quadratic convex optimization algorithm only needs 0.34 s and 0.5 s, respectively, a total of 0.84 s. However, IDE need to perform multiple iterations, and the calculation time is more than 400 minutes. Therefore, the proposed quadratic convex optimization method has low complexity and fast pattern synthesis compared with the global optimization algorithm.

4.1.3. Time Series Distribution Diagram. The radiation angle of the multiband is symmetrical with respect to the center position of the circular array. The switch sequence by the

proposed method presents the symmetry of the array elements. Table 2 shows the time series of circular array after using the quadratic convex optimization algorithm.

Comparing the time series of the 16-element circular array antenna with IDE, we can see the difference between the time series of the quadratic convex optimization algorithm and the IDE algorithm. The switch turn-on duration time of the array elements in the time series results in this paper is shorter than IDE, as shown in Figure 8.

4.1.4. Angular Scanning Characteristics of Circular Array Antenna. The multiband pattern by the proposed method can perform angular scanning. The pattern by IDE can only generate beams in a fixed radiation direction and cannot perform angular scanning.

When the $\varphi = 1°$, the peak level of the sidelobe at the center frequency band is -35.37 dB, the peak level of the sidelobe at the first-order sideband is -20.4 dB. When the $\varphi = 4°$, the peak level of the sidelobe at the center frequency band is -36.39 dB, and the peak level of the sidelobe at the first-order sideband is -22.2dB, although the sidelobe levels of the center frequency band and the first-order sideband have decreased. When the $\varphi = 4°$, the power in the main radiation direction can no longer meet the airspace radiation requirements. As the azimuth angle increases, the switch-on duration time of the array element gradually increases. The simulation results of the multiband pattern during azimuth scanning are shown in Figure 9. The time series results of the azimuth scanning are shown in Figure 10.

The simulation results when the circular array antenna changes the radiation azimuth angle φ show that when the radiation azimuth angle φ increases, the sidelobe levels of the center frequency band and the first-order sideband will decrease, but the energy in the main radiation direction no longer meets the given airspace radiation index. When the azimuth angle $\varphi = \pm 2°$, all 16 elements of the circular array antenna work. With the continuous increase of the azimuth angle scanning range, the working elements of the circular array antenna will decrease, so the performance of the multiband pattern will decrease, as shown in Figure 11.

Numerical results show that the performance of the multiband pattern synthesis is excellent when the circular array antenna radiates the azimuth angle $\varphi = 0°$. The pattern parameters of the azimuth scanning are given in Table 3.

4.1.5. Performance Analysis of Changing Beamwidth. The simulation results of the multiband pattern after changing the beamwidth (BW) of the circular array antenna are given in Figure 12. The time series results when the beamwidth is changed are shown in Figure 13.

When the BW = 7°, the peak sidelobe level of the center frequency band is -22.25 dB, and the peak sidelobe level of the first-order sideband is -23.4 dB. The peak sidelobe level of center frequency band increases 13.7 dB compared with BW = 10° . The peak level of the sidelobe becomes higher, and the performance of the antenna is not ideal. When the BW = 13°, the peak sidelobe level of the center frequency band is -46.91 dB, and the peak sidelobe level of the first-order sideband is -29.06 dB. Although the peak sidelobe level of the center frequency band and the first sideband is reduced compared with BW = 10°, the energy cannot be concentrated to the main lobe so that the detection performance of the target position and angle is reduced.

As the beamwidth continues to increase, the energy is more concentrated in the main radiation direction, but the accompanying wider bandwidth results in poorer target detection performance, as shown in Figure 14. The performance of changing BW is shown in Table 4.

4.2. Simulation of Satellite Array Antenna. The multiband pattern synthesis method of time-modulated conformal array antenna proposed in this paper can be used in the design of spaceborne antenna. This paper considers multiband pattern synthesis of time-modulated satellite array antenna.
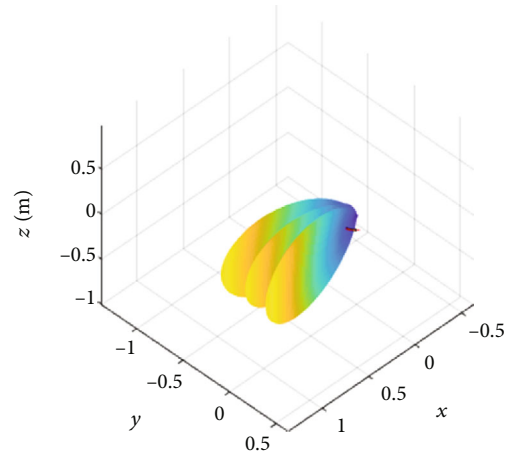

FIGURE 14: 3D pattern of the circular array when BW = 13°.

TABLE 4: Multiband pattern parameters when changing BW.

BW/°	4	7	10	13	16
SLL^0/dB	-2.57	-22.55	-36.25	-46.91	-54.13
SLL^1/dB	-12.16	-23.4	-18.71	-29.06	-32.91

4.2.1. Satellite Array Antenna Layout. This satellite array antenna is a six-sided cone composed of 276 array elements arranged at $\lambda/2$ equal intervals, and the default array element type is patch antenna. The array wavelength $\lambda = 0.024$m. The layout of the 276 array element satellite array antenna is shown in Figure 15.

4.2.2. Performance Analysis of Multiband Pattern of Satellite Array Antenna. The main radiation direction of the initialized satellite array antenna is $\varphi = 0°, \theta = 30°$. The quadratic convex optimization algorithm is used to realize the multiband pattern of the satellite array antenna in this paper, forming a beam with a peak sidelobe level of -40.98 dB at the center frequency band and forming a pencil beam with peak sidelobe level of -31.52 dB at the first-order sideband. The side lobe level of the satellite array antenna is effectively suppressed. The multiband pattern of the 276-element satellite array antenna is shown in Figure 16.

The 276-element satellite array antenna have six planes working at $\varphi = 0°, \theta = 30°$. The working state is shown in Figure 17.

4.2.3. Elevation Plane Scanning Characteristics of Satellite Array Antenna. The satellite array is angular scanning characteristics because of three-dimensional solid. The angular scanning characteristics of the satellite array antenna can show the spatial coverage ability of the antenna.

This paper considers elevation plane scanning of satellite array. Under the condition of fixed azimuth angle $\varphi = 0°$, changing the radiation elevation angle of the satellite array. When the $\theta = 25°$, the sidelobe level of the center frequency band is -43.82 dB, and the side lobe level of the first-order side band is -31.34 dB. When the $\theta = 75°$, the sidelobe level of the center frequency band is -20.56 dB, and the first-
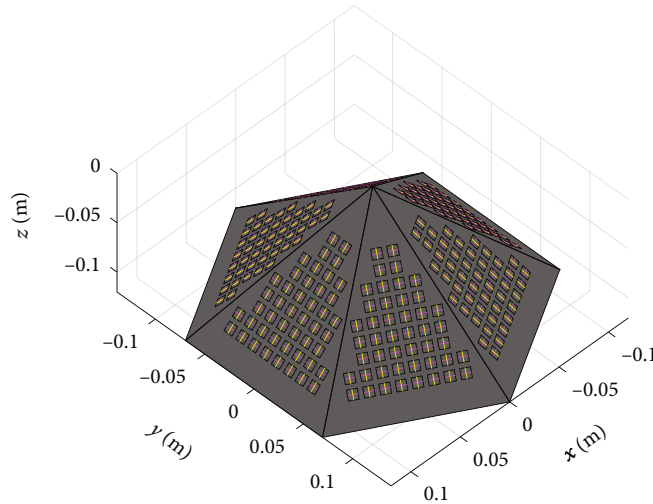
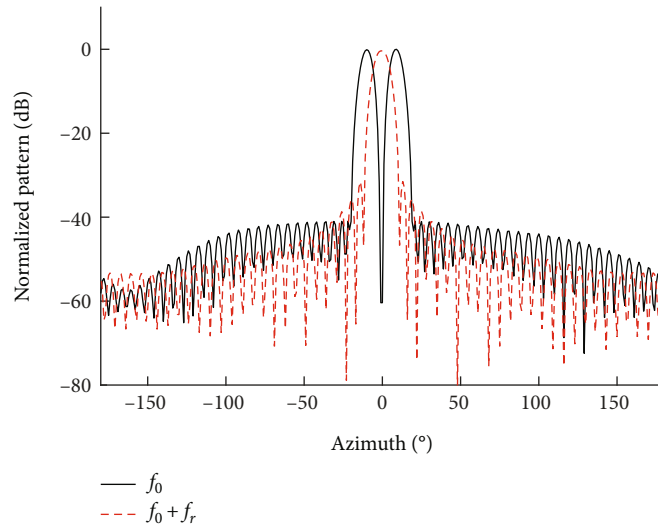FIGURE 15: The layout of satellite array antenna.

FIGURE 16: Multiband pattern of satellite array antenna.

order sideband side lobe level is -27.3 dB. At the same time, the distortion of the beam pattern is serious, the main radiation direction cannot meet the radiation requirements, and the suppression ability of the sidelobe is poor. The multiband pattern of satellite array by proposed method is obtained in Figure 18.

Under the condition of fixed azimuth angle $\varphi = 0°$, the satellite array antenna scanning characteristics show that when the elevation angle gradually from 0° to the normal vector direction of the array element, the beam sidelobe level of the satellite array antenna pattern gradually tend to be optimal. The elevation scanning characteristic of the satellite array antenna is excellent when the elevation angle is $[-50°, -20°]$ and $[20°, 50°]$. The elevation plane scanning performance is shown in Table 5.

When the radiation elevation angle is $[0°, 45°]$, the satellite array works on six faces. When the radiation elevation angle is $[46°, 63°]$, the satellite array works on five
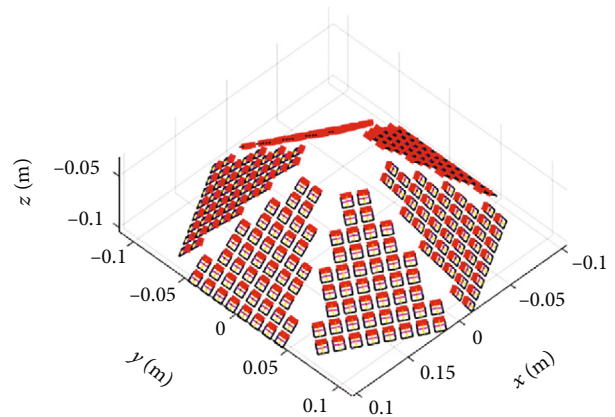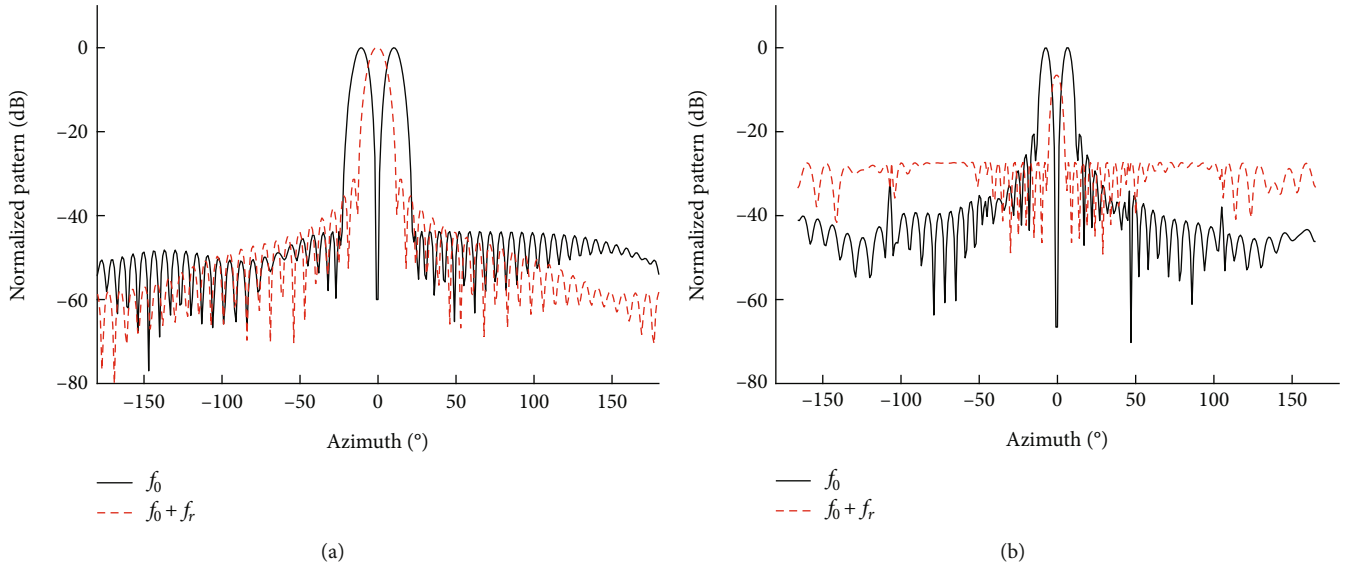

FIGURE 17: Six plane working states of the satellite array antenna at $\varphi = 0°, \theta = 30°$.

(a)

(b)

FIGURE 18: Multiband pattern of elevation plane scanning at (a) $\theta = 25°$ and (b) $\theta = 75°$.

TABLE 5: Scanning characteristics of elevation plane (θ).

$\theta/°$	5	15	25	35	45
SLL^0/dB	-136.3	-62.76	-43.82	-32.57	-29.3
SLL^1/dB	-84.3	-48.58	-31.34	-31.48	-32.08
$\theta/°$	55	65	75	85	90
SLL^0/dB	-35.89	-17.76	-20.56	-23.91	-17.98
SLL^1/dB	-45.26	-23.85	-27.3	-31.63	-41.33

faces. When the radiation elevation angle is $[64°, 90°]$, the satellite array antenna works on three planes, as shown in Figure 19.

4.2.4. Azimuth Plane Scanning Characteristics of Satellite Array Antenna.

This paper considers azimuth plane scanning of satellite array. In the case of a fixed radiation elevation angle $\theta = 30°$, changing the radiation azimuth of the satellite array, the multiband pattern of satellite array azimuth plane scanning by proposed method is obtained, as shown in Figure 20.

The satellite array antenna is a hexahedral pyramid with symmetry, so the azimuth angle scanning of the satellite array antenna only needs to consider the antenna performance of $[0°, 30°]$. When the $\varphi = 5°$, the side lobe level of the center frequency band is -48.48 dB, and the sidelobe level of the first-order side band is -45.38 dB. When the $\varphi = 25°$, the beam at the center frequency band is seriously distorted, and the first-order sideband beam cannot reach the spatial radiation index.

Under the condition of fixed elevation angle $\theta = 30°$, the satellite array antenna scanning characteristics show that when the azimuth angle gradually from 0° to 30°, the beam sidelobe level of the satellite array antenna pattern gradually tend to be worse. The azimuth scanning characteristic of the satellite array antenna is excellent when the azimuth angle is
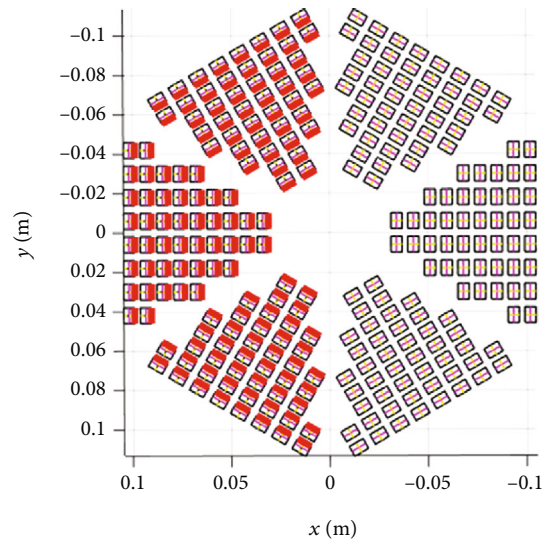

FIGURE 19: Three plane working states of the satellite array antenna.

$[-15°, 15°]$. When the radiation azimuth angle is $[0°, 30°]$, the satellite array works on six faces. The beam parameters of the pattern after azimuth plane scanning are shown in Table 6.

(a)

(b)
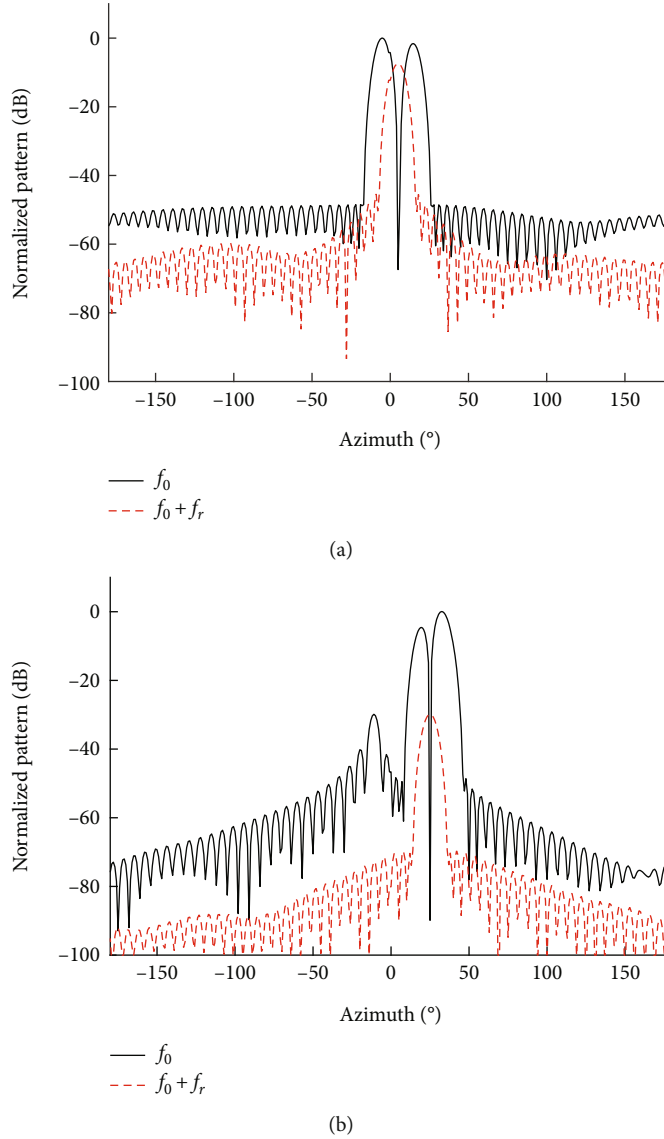
FIGURE 20: Multiband pattern of azimuth plane scanning at (a) $\varphi = 5°$ and (b) $\varphi = 25°$.

TABLE 6: Scanning characteristics of azimuth plane (φ).

$\varphi/°$	5	10	15	20	25	30
SLL^0/dB	-48.48	-53.32	-14.48	-11.76	-29.87	-33.59
SLL^1/dB	-45.38	-89.75	-61.8	-65.09	-69.77	-74.17

5. Conclusion

In this paper, a quadratic convex optimization algorithm for time-modulated conformal array multiband pattern synthesis is proposed. The proposed method can synthesize different beam and sum beam with low sidelobe level at the center frequency band and the first-order sideband, respectively, which solves the multiband pattern synthesis problem of complex time-modulated conformal arrays. The simulation results of the time-modulated circular and satellite array antenna show that the quadratic convex optimization algo-rithm has low sidelobe level and excellent angle scanning performance compared with IDE algorithm.

Data Availability

The data used to support the findings of this study are available from the corresponding author upon request.

Conflicts of Interest

The authors declare that they have no conflicts of interest.

Acknowledgments

References

[1] M. N. Sweeting, "Modern small satellites-changing the economics of space," *Proceedings of the IEEE*, vol. 106, no. 3, pp. 343–361, 2018.

[2] G. He, X. Gao, L. Sun, and R. Zhang, "A review of multibeam phased array antennas as LEO Satellite Constellation Ground Station," *IEEE Access*, vol. 9, pp. 147142–147154, 2021.

[3] B. J. Falkner, H. Zhou, A. Mehta, T. Arampatzis, D. Mirshekar-Syahkal, and H. Nakano, "A circularly polarized low-cost flat panel antenna array with a high impedance surface meta-substrate for satellite on-the-move medical IoT applications," *IEEE Transactions on Antennas and Propagation*, vol. 69, no. 9, pp. 6076–6081, 2021.

[4] B. P. Kumar, C. Kumar, V. S. Kumar, and V. V. Srinivasan, "Reliability considerations of spherical phased array antenna for satellites," *IEEE Transactions on Aerospace and Electronic Systems*, vol. 54, no. 3, pp. 1381–1391, 2018.

[5] K. A. Yinusa, "A dual-band conformal antenna for GNSS applications in small cylindrical structures," *IEEE Antennas and Wireless Propagation Letters*, vol. 17, no. 6, pp. 1056–1059, 2018.

[6] T. Pelham, G. Hilton, E. Mellios, and R. Lewis, "Predicting conformal aperture gain from 3-D aperture and platform models," *IEEE Antennas and Wireless Propagation Letters*, vol. 16, pp. 700–703, 2017.

[7] Y. Zeng, S. Zhang, N. Li et al., "Shaped elevation beam design for airborne conformal array detection," *IEEE Antennas and Wireless Propagation Letters*, vol. 19, no. 12, pp. 2192–2196, 2020.

[8] J. J. Peng, S. W. Qu, M. Xia, and S. Yang, "Conformal phased array antenna for unmanned aerial vehicle with ±70° scanning range," *IEEE Transactions on Antennas and Propagation*, vol. 69, no. 8, pp. 4580–4587, 2021.

[9] H. E. Shanks and R. W. Bickmore, "Four-dimensional electromagnetic radiators," *Canadian Journal of Physics*, vol. 37, no. 3, pp. 263–275, 1959.

[10] R. Maneiro-Catoira, J. Bregains, J. A. Garcia-Naya, and L. Castedo, "Analog beamforming with single-sideband sub-time-modulated arrays," in *2018 IEEE international symposium on antenna and propagation & USNC/URSI National Radio Science Meeting*, pp. 9-10, Boston, MA, USA, 2018.

[11] Y. Ma, C. Miao, Y. H. Li, and W. Wu, "A partition-based method for harmonic beamforming of time-modulated planar array," *IEEE Transactions on Antennas and Propagation*, vol. 69, no. 4, pp. 2112–2121, 2021.

[12] L. Poli, M. Salucci, D. Masotti, and P. Rocca, "Optimization-based synthesis of time-modulated arrays with accurate time-frequency analysis," in *2019 27th European Signal Processing Conference (EUSIPCO)*, pp. 1–4, A Coruna, Spain, 2019.

[13] Z. J. Jiang, S. Zhao, Y. Chen, and T. J. Cui, "Beamforming optimization for time-modulated circular-aperture grid array with DE algorithm," *IEEE Antennas and Wireless Propagation Letters*, vol. 17, no. 12, pp. 2434–2438, 2018.

[14] M. A. Panduro, A. L. Mendez, R. Dominguez, and G. Romero, "Design of non-uniform circular antenna arrays for side lobe reduction using the method of genetic algorithms," *AEU-International Journal of Electronics and Communications*, vol. 60, no. 10, pp. 713–717, 2006.

[15] Z. K. Zhang, L. J. Sun, and L. Xu, "Multiple beamforming with null steering based on improved invasive weed optimization," in *2020 12th International Conference on Knowledge and Smart Technology (KST)*, pp. 36–40, Pattaya, Thailand, 2020.

[16] J. Yang, W. Li, and X. Shi, "Pattern synthesis of time-modulated conformal arrays by an improved differential evolution algorithm," *International Journal of RF and Microwave Computer-Aided Engineering*, vol. 24, no. 6, pp. 697–705, 2014.

[17] A. Mukherjee, S. K. Mandal, and R. Ghatak, "Differential evolution to synthesize low sidelobe thinned isophoric time- modulated planar array with increased directivity," *International Journal of RF and Microwave Computer-Aided Engineering*, vol. 29, no. 11, 2019.

[18] A. Reyna Maldonado and M. A. Panduro, "Synthesis of concentric ring antenna array for a wide isoflux pattern," *International Journal of Numerical Modelling: Electronic Networks, Devices and Fields*, vol. 28, no. 4, pp. 433–441, 2015.

[19] T. Hong, X. P. Shi, and X. S. Liang, "Synthesis of sparse linear array for directional modulation via convex optimization," *IEEE Transactions on Antennas and Propagation*, vol. 66, no. 8, pp. 3959–3972, 2018.

[20] Y. X. Zhang, Y. C. Jiao, and L. Zhang, "Antenna array directivity maximization with sidelobe level constraints using convex optimization," *IEEE Transactions on Antennas and Propagation*, vol. 69, no. 4, pp. 2041–2052, 2021.

[21] Z. X. Huang and Y. J. Cheng, "Near-field pattern synthesis for sparse focusing antenna arrays based on Bayesian compressive sensing and convex optimization," *IEEE Transactions on Antennas and Propagation*, vol. 66, no. 10, pp. 5249–5257, 2018.

[22] G. Prisco and M. D'Urso, "Maximally sparse arrays via sequential convex optimizations," *IEEE Antennas and Wireless Propagation Letters*, vol. 11, pp. 192–195, 2012.

[23] Z. Qi, Y. Bai, and X. Zhang, "Synthesis of linear and planar arrays via sequential convex optimizations," *IEEE Access*, vol. 8, pp. 6717–6728, 2020.

[24] K. Tang and X. Zhang, "Auto-determining mainlobe width for beampattern synthesis via relaxation optimization," *IEEE Signal Processing Letters*, vol. 29, pp. 314–318, 2022.

[25] C. Yang, N. Ou, Y. Deng et al., "Pattern synthesis algorithm for range ambiguity suppression in the LT-1 mission via sequential convex optimizations," *IEEE Transactions on Geoscience and Remote Sensing*, vol. 60, pp. 1–13, 2022.

[26] F. Yang, S. Yang, Y. Chen, S. Qu, and J. Hu, "Efficient pencil beam synthesis in 4-D antenna arrays using an iterative convex optimization algorithm," *IEEE Transactions on Antennas and Propagation*, vol. 67, no. 11, pp. 6847–6858, 2019.

[27] Y. Gong, S. Xiao, and B. Wang, "Synthesis of nonuniformly spaced arrays with frequency-invariant shaped patterns by sequential convex optimization," *IEEE Antennas and Wireless Propagation Letters*, vol. 19, no. 7, pp. 1093–1097, 2020.

[28] Y. Aslan, J. Puskely, A. Roederer, and A. Yarovoy, "Multiple beam synthesis of passively cooled 5G planar arrays using convex optimization," *IEEE Transactions on Antennas and Propagation*, vol. 68, no. 5, pp. 3557–3566, 2020.

[29] H. Luan, C. Chen, W. Chen, L. Zhou, H. Zhang, and Z. Zhang, "Mutual coupling reduction of Closely E/H-Plane coupled antennas through metasurfaces," *IEEE Antennas and Wireless Propagation Letters*, vol. 18, no. 10, pp. 1996–2000, 2019.

[30] Y. Liu, Y. Yang, P. Wu et al., "Synthesis of multibeam sparse circular-arc antenna arrays employing refined extended alternating convex optimization," *IEEE Transactions on Antennas and Propagation*, vol. 69, no. 1, pp. 566–571, 2021.